A Dynamic ^{15}N NMR Study of Kinetic Hydrogen/Deuterium Isotope and Tunnel Effects on the Triple Proton Transfer in Crystalline 3,5-Dimethylpyrazole

Francisco Aguilar-Parrilla[1,*], Oliver Klein[2], José Elguero[2], and Hans-Heinrich Limbach[1,]**

[1]) Institut für Organische Chemie, Freie Universität Berlin, Takustrasse 3, D-14195 Berlin, Germany
[2]) Instituto de Química Médica, CSIC, Juan de la Cierva 3, E-28006 Madrid, Spain

Key Words: Crystals / Hydrogen Bonding / Isotopes / Proton Transfer / Spectroscopy, Nuclear Magnetic Resonance

Using dynamic solid state ^{15}N CPMAS NMR spectroscopy (CP≡cross polarization, MAS≡magic angle spinning) the kinetics of the degenerate intermolecular triple proton and deuteron transfer in the cyclic trimers of ^{15}N-labeled polycrystalline 3,5-dimethylpyrazole (DMP) have been studied in a wide temperature range. At high temperatures, rate constants of the various isotopic HHH, HHD, HDD, and DDD transfer reactions are obtained in the millisecond timescale by lineshape analysis of partially deuterated doubly ^{15}N-labeled DMP. At low temperatures, the kinetics were followed by magnetization transfer methods in the laboratory frame. In order to suppress artifacts arising from ^{15}N-spin diffusion these experiments were performed on singly ^{15}N labeled DMP, partially diluted in the non-labeled material. As multiple kinetic hydrogen/deuterium isotope effects on triple proton transfer reactions have not yet been studied these effects are modeled theoretically for the single barrier case involving a concerted proton motion and for the triple barrier case where the three protons are transferred stepwise. The experimental kinetic isotope effects obey the rule of the geometric mean, i.e. $k^{HHH}/k^{HHD} \approx k^{HHD}/k^{HDD} \approx k^{HDD}/k^{DDD} \approx 3.6$ i.e. $\approx k^{HHH}/k^{DDD} \approx 47$ at 300 K, which is indicative of a single barrier where all hydrons loose zero-point energy in the transition state. At low temperatures, strong deviations from an Arrhenius behavior are observed for all isotopic reactions, indicating incoherent triple hydron tunneling processes, which are described in terms of a modified Bell tunneling model.

1. Introduction

In the past years dynamic variable temperature ^{15}N CPMAS NMR spectroscopy (CP≡cross polarization, MAS≡magic angle spinning) of ^{15}N-labeled heterocyclic compounds has been shown to be a convenient method in order to follow the kinetics of intramolecular double [1] and single proton transfer reactions [2]. Recently, it was shown that this method could also be used for the determination of kinetic hydrogen/deuterium isotope effects from which interesting information about the reaction mechanism is obtained [3, 4]. For example, in the case of the double proton transfer in solid porphyrin [1k] the transfer was shown to be stepwise involving tunneling at low temperatures. The stepwise mechanism was shown to be a consequence of the properties of the porphyrin skeleton which does not allow the simultaneous formation and compression of two cooperative intramolecular NH···N hydrogen bonds. By contrast, this phenomenon can occur in the case of intermolecular double proton transfer systems [4]. Unfortunately, until recently intermolecular solid state double proton transfers which could by studied be NMR were rare. Exceptions are the cyclic dimers of carboxylic acids (Fig. 1a) whose tautomerism including kinetic HH/HD/DD isotope effects were studied using ^1H and ^2H solid state NMR relaxometry [5], and very recently the case of diarylformamidines (Fig. 1b) [6]. These studies indeed indicated concerted double proton transfers involving tunneling at low temperatures, as was proposed also in the case of some liquid state double proton transfers [4].

Some time ago a most versatile series of intermolecular multiple proton transfer systems was proposed by Elguero et al. [7], i.e. substituted pyrazoles (Fig. 1c) which can be regarded as molecular synthons in order to build up various supramolecular hydrogen-bonded structures, such as linear chains, helices and cyclic hydrogen-bonded dimers, trimers, tetramers etc. The structure and multiple proton dynamics of solid pyrazoles have been studied by a combination of x-ray crystallography and solid state NMR methods [7a–p] as well as by ab-initio quantum-mechanical calculations [7p]. Depending on the substituents degenerate double, triple or quadruple proton transfers have been observed. Thus, these systems constitute an interesting series of compounds where the influence of the number of protons transferred on the reaction mechanism can be studied. E.g., it seems possible that the proton transfer is concerted for a small number of protons transferred but stepwise when this number becomes larger [7p]. Therefore, pyrazoles constitute in a similar way as hydrogen-bonded associates of HF [8] interesting model systems for multiple proton transfer even in protic environments.

In this paper we are concerned with the degenerate triple proton transfer in solid 3,5-dimethylpyrazole (DMP), the first compound in this series which was shown by solid state NMR to exhibit a degenerate solid state triple proton tautomerism [7a,b,c,f]. DMP crystallizes in columns of cyclic trimers (Fig. 2a,b), and the dynamic disorder arising from the degenerate tautomerism leads to an effective x-ray D_{3h} symmetry where all nitrogen atoms are characterized by a formal average proton density of $\frac{1}{2}$. Using ^{15}N NMR some preliminary kinetic HHH/DDD isotope effects have been observed which were larger than 20 at room temperature [7b]. In addition, at low temperatures, evidence for a

*) Present address: Schering AG, D-13342 Berlin, Germany.
**) Author to whom correspondence should be addressed.

  0005-9021/97/0606-889 $ 15.00+.25/0

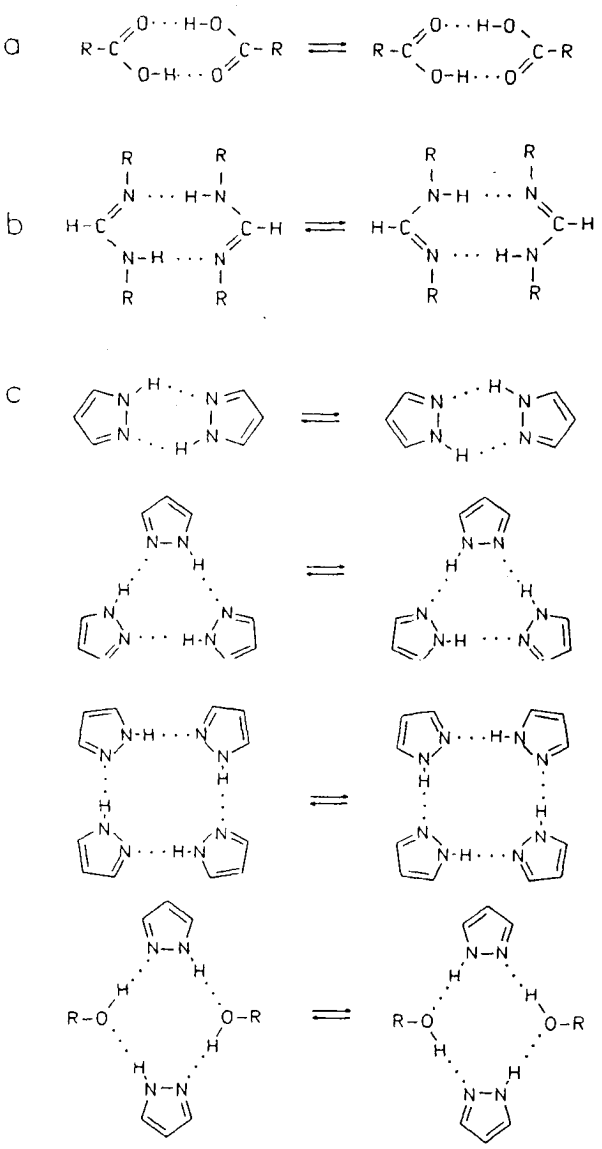

Fig. 1
Intermolecular multiple proton transfer reactions in solids. (a) Cyclic dimers of carboxylic acids. (b) Cyclic formamidine dimers. (c) Cyclic dimers, trimers and tetramers of pyrazole derivatives

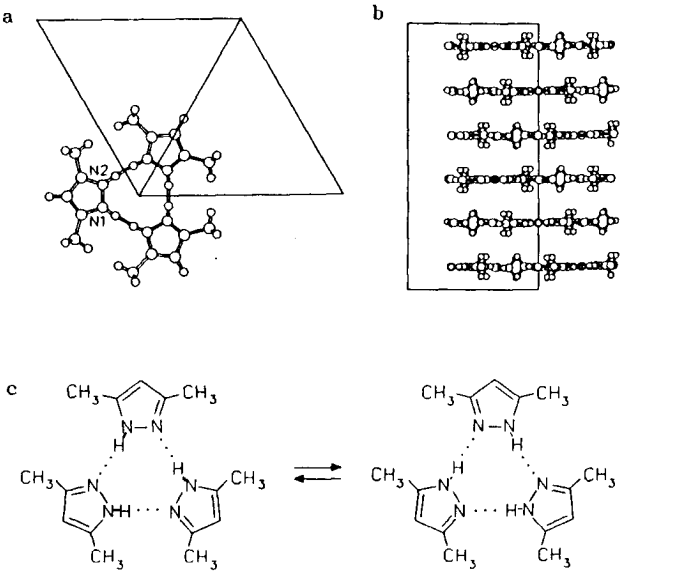

Fig. 2
The crystal structure of DMP according to Ref. [7a]. The compound crystallizes in the $R\bar{3}c$ space group. (a) View of the cyclic trimer projected along the *c* axis. (b) Molecular packing view projected along the *b* axis showing the planarity of the trimer. (c) Schematic representation of the triple proton transfer in solid DMP

non-Arrhenius behavior of the triple proton transfer was obtained [7c]. These results incited us, therefore, to study the full kinetic HHH/HHD/HDD/DDD isotope effects in a large temperature range, because such effects have not yet been described; their knowledge seemed us desirable in order to elucidate the reaction mechanism in the case of DMP and to advance the theory of kinetic hydrogen/deuterium isotope effects. It will be shown that these isotope effects provide evidence for a single barrier process involving a compressed transition state where all mobile protons have lost considerable zero-point energies. At low temperatures tunneling becomes visible in the Arrhenius curves of all isotopic reactions, simulated in terms of a tunneling model based on the Bell model [9].

In this paper we, therefore, report the results of a study of the full multiple hydrogen/deuterium isotope effects in crystalline DMP. For this purpose, ^{15}N CPMAS NMR experiments were performed on doubly and singly ^{15}N-labeled and partially deuterated polycrystalline DMP which include lineshape analysis as well as magnetization transfer experiments which have been shown to provide rate constants in the millisecond to second timescale [1g]. The ^{15}N isotopic dilution experiments were necessary in order to exclude ^{15}N spin diffusion mediated by protons [1g, 10].

The paper is organized as follows. After an experimental section we present the results of the dynamic NMR experiments used as a tool to study the multiple kinetic isotope effects of the tautomerism of DMP in the solid state. On the basis of these results the mechanism of the transfer process is then discussed. For this purpose predictions of kinetic isotope effects for synchronous and stepwise jumps of three protons in the absence and presence of tunneling are derived.

2. Experimental Section

2.1 Materials

DMP-$^{15}N_2$ **1** was synthesized according to procedures reported in the literature starting from doubly ^{15}N-labeled hydrazine sulfate [11]. The singly labeled compound DMP-^{14}N-^{15}N **2** was prepared in a similar way using singly ^{15}N-labeled hydrazine sulfate. The latter was synthesized starting from $^{15}NH_3$ and hydroxylamine-O-sulphonic acid [12]. Dilute samples of **2** were prepared by dissolving desired quantities of DMP-^{14}N-^{15}N and DMP-$^{14}N_2$ in diethylether followed by evaporation of the solvent.

The desired deuterium fractions x_D in the mobile proton sites **1** were achieved by mixing CH_3OD as deuterating agent and CH_3OH in the corresponding amounts under argon atmosphere followed by evaporation of the solvent in vacuo.

2.2 ^{15}N CPMAS NMR Measurements

The ^{15}N-CPMAS-NMR experiments were performed using Bruker CXP 100 (2.1 Tesla, 90.02 MHz for ^{1}H and 9.12 MHz for ^{15}N, 7 mm Doty standard CPMAS probe) and Bruker MSL 300 (2.1 Tesla, 300.13 MHz for ^{1}H and 30.41 MHz for ^{15}N, 5 mm high speed Doty CPMAS probe) spectrometers. For both spectrometers spinning speeds were so high (2.5 and 9 kHz) that rotational side bandes could be avoided. Because of sample heating in the case of the high speed probe [13], a small quantity of ^{15}N-labeled tetramethyltetraaza[14]annulene (TTAA) was added in a separate capsule into the high-speed 5 mm rotors in order to obtain the sample temperatures from the temperature-dependent ^{15}N chemical shifts of TTAA [7f, 13]. In the case of the standard CPMAS probe the sample temperatures were measured using a PT-100 platinum resistance thermometer placed inside the gas supply close to the stator. On both spectrometers a Bruker B-VT-1000 temperature unit was used to control the temperature of the bearing gas stream and a home-built heat exchanger [14] to achieve low temperatures. Throughout this study pure nitrogen was used as bearing and driving gas. All chemical shifts are related to external solid $^{15}NH_4Cl$ and given with an error of ± 0.3 ppm.

Standard CPMAS spectra were measured using the usual CP pulse sequence [15] and the lineshape analyses done as described previously [3a]. The magnetization transfer experiments in the laboratory frame between the amino nitrogen magnetization S and the imino nitrogen magnetization X were performed using a sequence described previously [1g, 9]. In these experiments S and X are created by cross polarization and stored by 90° pulses parallel to the magnetic field B_0. The time dependence during this period is monitored after application of a second 90° pulse. The dependence is given by [1g]

$$S+X=(S_0+X_0)\exp(-\rho t)\ ,$$
$$S-X=(S_0-X_0)\exp(-(\rho+\sigma+2k)t)\ , \qquad (1)$$

where $\rho = 1/T_1$ represents the longitudinal relaxation rate, σ the rate of spin diffusion between S and X, and k the rate constant of the degenerate exchange between the two sites [1g]. Two experiments are performed by setting a time interval t_1 between the spin lock pulses and the 90° pulse either to 0 or to $1/2(\nu_S-\nu_X)$, where ν_S and ν_X represent the chemical shifts in Hz of the exchanging sites. In the "parallel" experiment (i) S_0 and X_0 have the same sign and are almost equal. Therefore $S-X=0$ and S and X each decay with the longitudinal relaxation rate ρ. In the "antiparallel" experiment (ii) S_0 and X_0 are antiparallel, i.e. $S_0 \approx -X_0$, and each magnetization decays with $\rho+\sigma+2k$ in time. As ρ is already known from experiment (i) the sum $\sigma+2k$ is obtained in experiment (ii). Various stratagems have been proposed in order to obtain σ and k separately. Here we exploit the circumstance that σ is strongly dependent on the distance between the ^{15}N nuclei in contrast to k. Thus, σ could be minimized by performing the magnetization transfer experiments on singly ^{15}N-labeled DMP instead of using the doubly labeled material.

3. Results

In this section we report the results of the dynamic ^{15}N CPMAS NMR experiments performed on polycrystalline DMP as a function of the deuterium fraction x_D in the mobile proton sites. At $x_D>0$ cyclic trimers containing the mobile hydron combinations HHH, HHD, HDD, and DDD are present in a polycrystalline sample. In the case of a statistic isotopic distribution the mole fractions of the various isotopomers are given by

$$x_{HHH}=(1-x_D)^3\ ,\quad x_{HHD}=3(1-x_D)^2x_D\ ,$$
$$x_{HDD}=3(1-x_D)x_D^2\ ,\quad x_{DDD}=x_D^3 \qquad (2)$$

and are depicted in Fig. 3 as a function of x_D. In principle, the rate constant k^{LLL} of the triple hydron transfer in a given isotopomeric trimer could depend on the isotopic composition of the surrounding trimers. However, we did not find any evidence in this study for such a dependence. Therefore, we treat polycrystalline samples of DMP at deuterium fractions $x_D>0$ as a statistical static mixture of the various independent isotopomeric trimers LLL, each characterized by a single triple hydron transfer rate constant k^{LLL}.

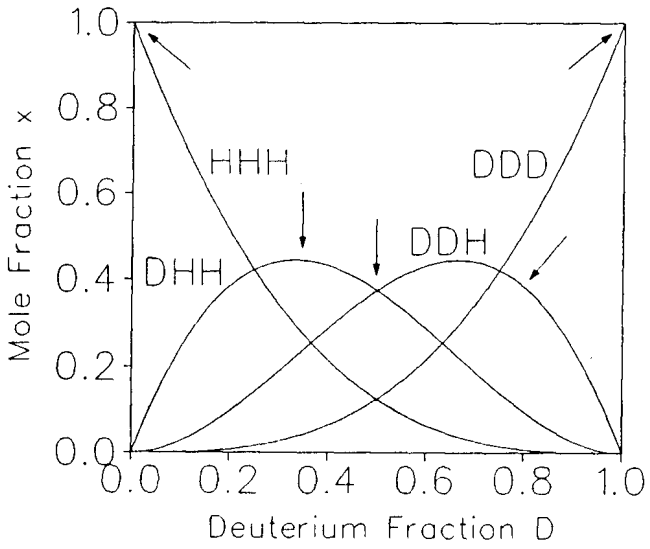

Fig. 3
Mole fractions of the isotopomeric trimers HHH, HHD, HDD, and DDD calculated for a statistical distribution according to Eq. (2)

In the following, we firstly describe the determination of the rate constants of the isotopic reactions around and below room temperature using ^{15}N CPMAS NMR lineshape analysis. Then the results of the magnetization transfer experiments performed at low temperatures are reported. All kinetic data obtained are assembled in Tables 1 and 2.

Table 1
Rate constants of the proton and deuteron transfer in polycrystalline DMP obtained by ^{15}N CPMAS NMR lineshape analysis

T/K	k^{HHH}	T/K	k^{HHH}	T/K	k^{HHD}	T/K	k^{HDD}	T/K	k^{DDD}
291	650	323	4050	318	820	318	260	331	220
300	990	326	4950	328	1700	328	500	347	620
302	1100	328	5600	333	2370	333	780	354	870
306	1450	332	6900	340	3400	340	1100	361	1250
309	1850	336	8800	345	4400	345	1500		
313	2350	340	10600	350	5400	350	2100		
320	3400	344	13100	356	7500	356	2900		
				364	12100	364	4400		

Table 2
Rate constants of the triple proton transfer in polycrystalline DMP obtained by ^{15}N-magnetization transfer experiments at 30.41 MHz on singly ^{15}N-labeled DMP at $x_D = 0$

T/K	k^{HHH}/s^{-1}	T/K	k^{HHH}/s^{-1}	T/K	k^{HHH}/s^{-1}	T/K	k^{HHH}/s^{-1}
130	0.017[a])	230	13.4[a])	122	0.019[b])	175	0.27[c])
131	0.022[a])	240	28[a])	129	0.019[b])	185	0.51[c])
158	0.09[a])	249	53[a])			193	0.96[c])
196	1.5[a])	261	107[a])			203	1.8[c])
208	2.8[a])	272	175[a])				

[a]) 100% singly labeled DMP
[b]) 35% singly labeled DMP
[c]) 10% singly labeled DMP

Table 3
Rate constants of the triple hydron transfer in polycrystalline DMP obtained by ^{15}N-magnetization transfer experiments at 30.41 MHz on singly ^{15}N-labeled DMP at various deuterium fractions x_D

T/K	k^{HHH}/s^{-1}	k^{HHD}/s^{-1}	T/K	k^{HDD}/s^{-1}	k^{DDD}/s^{-1}
160	0.08	0.006	211	0.06	0.005
177	0.27	0.017	222	0.085	0.027
190	1	0.04	230	0.3	0.045
200	1.8	0.05	231	0.25	0.044
210	2.65	0.08	238	0.5	0.08
220	5.58	0.21	240	0.4	0.15
229	7.8	0.45	241	0.4	0.16
			253	2.0	0.33
			262	5.0	1.0
			274	7.9	2.3
			286	24	7.2

k^{HHH} and k^{HHD} were obtained from a sample with $x_D = 0.2$ and k^{HDD} and k^{DDD} from a sample with $x_D = 0.8$

Table 4
Summary of kinetic results of the triple hydron transfer in polycrystalline 3,5-dimethylpyrazole

LLL	$\log A^L$	E_a^{LLL}	T_{min}	T_{max}		300 K		300 K
HHH	2.5	10.0	111	166	k^{HHH}	1016	k^{HHH}/k^{DDD}	47
	4	13.3	190	230				
	9.4	35.9	230	290				
	11.5	53.6	291	344				
HHD	3.54	18	160	229	k^{HHD}	270.5	k^{HHH}/k^{HHD}	3.8
	11.5	55.8	318	364				
HDD	9.7	45.6	222	238	k^{HDD}	73.5	k^{HHD}/k^{HDD}	3.7
	11.5	57.0	318	364				
DDD	9.5	47.9	222	286	k^{HDD}	21.6	k^{HDD}/k^{DDD}	3.4
	11.5	59.9	274	361				

Frequency factors A^{LLL} in s^{-1}, activation energies E_a^{LLL} in kJ mol^{-1}, k^{LLL} rate constants of triple hydron transfer in s^{-1}, T_{min}, T_{max} temperature range

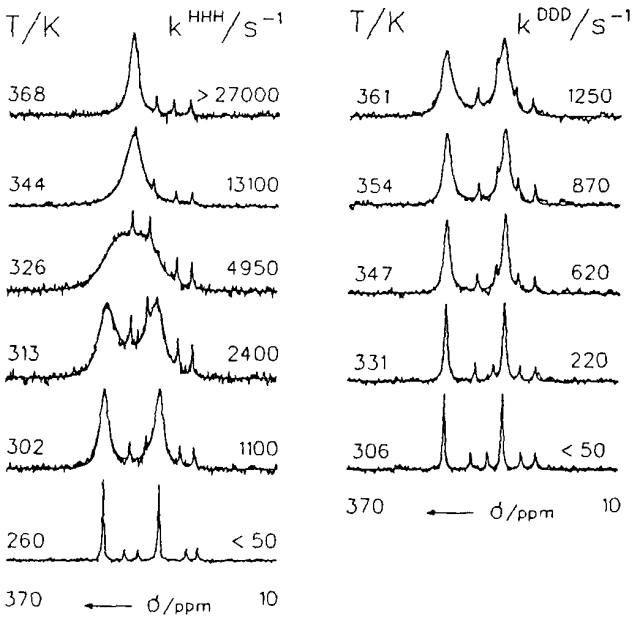

Fig. 4
Superposed experimental and calculated 30.41 MHz (7 Tesla) ^{15}N CPMAS-NMR spectra of 95% ^{15}N-enriched DMP at the deuterium fractions $x_D = 0$ (a) and $x_D = 1$ (b) as a function of the temperature. Experimental conditions: 8 – 9 kHz sample spinning, 6 – 12 ms CP times, 4.3 s repetition time, 5 μs ^1H 90° pulses, k^{HHH} and k^{DDD} are the rate constant of the triple proton and deuteron transfer. The four sharp lines with temperature-dependent line positions stem from a small quantity of ^{15}N-labeled tetramethyltetraaza[14]annulene (TTAA) added in a separate capsule. The line positions directly calibrate the internal temperature of the sample inside the rotor [13].

3.1 ^{15}N CPMAS NMR Lineshape Analysis

3.1.1 Determination of k^{HHH} and k^{DDD}

In a first stage, spectra of DMP were measured and analyzed at $x_D = 0$ and 1 at different temperatures in order to obtain k^{HHH} and k^{DDD}. Some 30.41 MHz ^{15}N CPMAS NMR spectra are shown in Fig. 4. As reported already in Refs. [7b, f], at low temperature two signals are observed at 166.8 and 241.3 ppm for the amino-(–NH–, –ND–) and imino-(–N=) nitrogen atom sites. As the cross polarization dynamics of nuclei in different chemical sites are different [16] which can lead to signal intensity distortions in the resulting spectra, the cross polarization times t_{CP} used in the experiments were adjusted in such a way that the signals of the amino and imino nitrogen atoms sites were equal. We note that small differences are also averaged out by magnetization transfer arising from the tautomerism as discussed below. As temperature is increased, the lines

broaden and coalesce at $x_D = 0$ around room temperature, where still two fairly sharp lines are obtained at $x_D = 1$. Around 360 K only one fairly sharp line is observed at $x_D = 0$ and a two broadened line at $x_D = 1$. The observation that the coalesced line at $x_D = 0$ appears midway between the two low temperature signals indicates that all nitrogen atoms have an equal proton density of 0.5, i.e. that the equilibrium constant of the triple proton transfer $K = 1$ within the margin of error. These observations confirm the presence of a large primary isotope effect k^{HHH}/k^{DDD} already detected at 2.1 Tesla [7b]. The rate constant were determined by lineshape analysis using the usual two-site theory [3a] and the agreement between the experimental and calculated spectra is very satisfactory, as indicated in Fig. 4.

3.1.2 Determination of k^{HHD} and k^{HDD}

The total ^{15}N NMR lineshapes can be decomposed into a sum of four independent lineshape contributions for each isotopomeric trimer LLL, characterized by the rate constant k^{LLL} and the mole fraction x_{LLL} which can be calculated from the value of x_D according to Eq. (2). Thus, as x_D is known approximately from the sample preparation and as k^{HHH} and k^{DDD} were already known, the only remaining two unknown parameters determining the lineshapes are k^{HHD} and k^{HDD}, if lineshape distortions arising from different cross-polarization dynamics of the ^{15}N nuclei in the protonated and deuterated $^{15}N\text{-}H\cdots{}^{15}N$ and $^{15}N\text{-}D\cdots{}^{15}N$ hydrogen bonds are eliminated. This goal was achieved as follows. Equal amounts of DMP with deuterium fractions $x_D = 0$ and 1 were placed in a rotor constituting a sample with $x_{HHH} = x_{DDD} = 0.5$. The ^{15}N CPMAS spectra of this sample were recorded between 300 and 350 K, under variation of the cross polarization times t_{CP}. For each temperature, a value of t_{CP} could be found where the correct mole fractions were obtained by lineshape analysis, using the known values of k^{HHH} and k^{DDD}. An example referring to 318 K is depicted in Fig. 5 where the optimum value of t_{CP} was 10 ms. This procedure was repeated at different temperatures, and the resulting optimized spectra of this sample are shown in Fig. 6a.

For the remaining experiments carried out on samples with varying deuterium fractions x_D now the optimized t_{CP} values were employed. The resulting superposed experimental and calculated spectra are shown in Fig. 6b – d. Now the lineshape contributions of the $^{15}N\text{-}H\cdots{}^{15}N$ and the $^{15}N\text{-}D\cdots{}^{15}N$ units in a given isotopomer LLL = HHD, HDD are the same as they depend on the same rate constants k^{LLL}. Thus, only the parameters k^{HHD} and k^{HDD} needed to be varied in the lineshape analysis. As there are some small deuterium losses during the sample preparation x_D was also allowed to be varied slightly, but the best parameter values listed in Fig. 6 were then kept constant for a given sample. In principle, the spectra of Fig. 6b – d were simulated simultaneously, and the individual lineshape contributions of the various isotopic species are depicted in Fig. 6e – h. As mentioned above the lineshapes of Fig. 6a

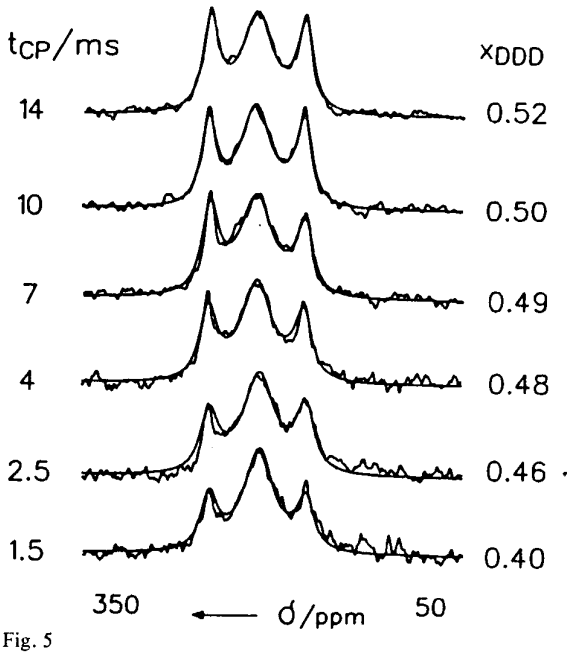

Fig. 5
9.12 MHz superposed experimental and calculated ^{15}N CPMAS-NMR spectra at 318 K of a sample containing separately equal parts of DMP with a deuterium fraction of $x_D = 0$ and 1. The cross polarization times t_{CP} were varied and the spectra analyzed using the known values of k^{HHH} and k^{DDD} by varying the effective mole fraction $x_{DDD} = 1 - x_{HHH}$. The correct value 0.5 was obtained at $t_{CP} = 10$ ms

consist of equal contributions from the lineshape of the HHH trimers (Fig. 6e) and the DDD trimers (Fig. 6h), i.e. $x_{HHH} : x_{DDD} = 0.5 : 0.5$. In Fig. 6c the total deuterium content is the same, however, now $x_{HHH} : x_{HHD} : x_{HDD} : x_{DDD} = 0.125 : 0.375 : 0.375 : 0.125$, i.e. HHD and HDD dominate and lead to completely different lineshape than in Fig. 6a. At $x_D = 0.8$ where $x_{HHH} : x_{HDD} : x_{HDD} : x_{DDD} = 0.008 : 0.096, 0.384 : 0.512$ the HDD and DDD trimers dominate the lineshapes, as can be inferred by comparison of Fig. 6d with g and h. At $x_D = 0.35$ (Fig. 6b) where $x_{HHH} : x_{HHD} : x_{HDD} : x_{DDD} = 0.275 : 0.404 : 0.239 : 0.043$ the dominating species is HHD.

3.2 ^{15}N CPMAS NMR Magnetization Transfer Experiments

3.2.1 Determination of k^{HHH} and k^{DDD}

Since at low temperatures the reaction rates are too small to be determined accurately enough by lineshape analysis, one-dimensional ^{15}N CPMAS magnetization transfer were performed. In order to estimate and suppress the ^{15}N spin diffusion term σ in Eq. (1) we performed the following ^{15}N dilution experiments. Firstly, experiments were performed at $x_D = 0$ on doubly and then on singly (95%) ^{15}N-labeled DMP. We obtained slightly smaller decay constants $\sigma^{HHH} + 2k^{HHH}$ in the case of the latter sample indicating that σ^{HHH} had been reduced as the internuclear distances between ^{15}N nuclei was increased substantially. Then we prepared samples where singly ^{15}N-labeled DMP was

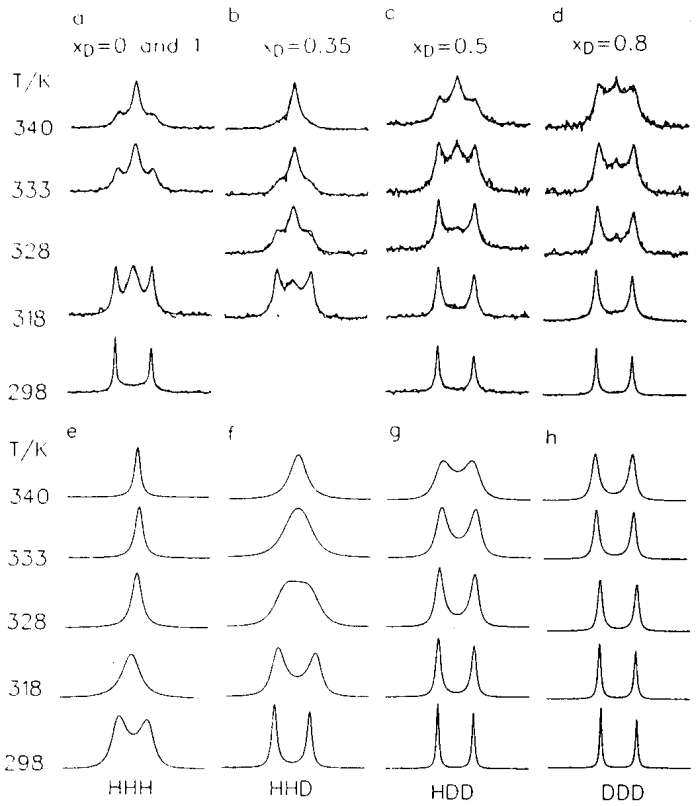

Fig. 6
Superposed experimental and calculated 9.12 MHz ^{15}N CPMAS-NMR spectra of doubly ^{15}N-labeled DMP as a function of the deuterium fraction x_D in the mobile proton sites and of temperature. (a) Spectra of the sample of Fig. 3 with $x_{HHH} = x_{DDD} = 0.5$ where the values of t_{CP} = 7, 10, 12, 14, 16, 18 ms at 298, 318, 328, 333, 340, and 345 K were adjusted in such a way that the correct mole fractions were obtained. (b) to (d) Spectra of DMP with varying deuterium fractions of x_D. (e) to (f) Calculated subspectra of HHH, HHD, HDD, and DDD trimeric isotopomers. ^{15}N chemical shift scale as in Fig. 5

embedded in non-labeled DMP to about 35 and 10% and repeated the magnetization transfer experiments. However, we but could not find any significant changes of the decay constants down to the lowest temperatures of about 120 K where experiments were performed. Thus, all further experiments at varying deuterium fractions x_D were performed on the singly (95%) ^{15}N-labeled material, and the analysis carried out neglecting the spin diffusion term in Eq. (1). Taking into account the different isotopic species this equation can then be rewritten as

$$S+X = \sum_{LLL} C_{LLL} \exp(-\rho^{LLL} t) ,$$

$$S-X = \sum_{LLL} D_{LLL} \exp(-(\rho^{LLL} + 2k^{LLL}) t) \qquad (3)$$

where LLL = HHH, HHD, HDD, DDD. The coefficients C_{LLL} and D_{LLL} are equal to the mole fractions x_{LLL} in the absence of signal intensity distortions arising from different cross polarization dynamics in the different isotopomeric trimers. However, as these coefficients could be directly obtained by non-linear least squares fitting there was no need for an adjustment of the cross polarization times t_{CP} as in the lineshape experiments.

In Fig. 7 the results of a typical experiment carried out at 30.41 MHz at 131 K and spinning speeds of about 8 to 9 kHz on singly ^{15}N-labeled DMP are depicted. The sample temperatures were obtained from the four lines of added ^{15}N-enriched TTAA as described in the experimental section. Fig. 7a shows the results of experiment (i) performed at $x_D = 0$. No variation of the magnetizations within the time period covered is observed indicating that ρ^{HHH} is so small that it can be neglected. In experiment (ii) performed on the same sample under otherwise similar conditions the two magnetizations cancel each other in the same time period because of the triple proton transfer. For comparison, the results of experiment (ii) on a sample with $x_D = 1$ are shown in Fig. 7c; no change of the magnetization is observed as the DDD process is very slow. The analysis of the

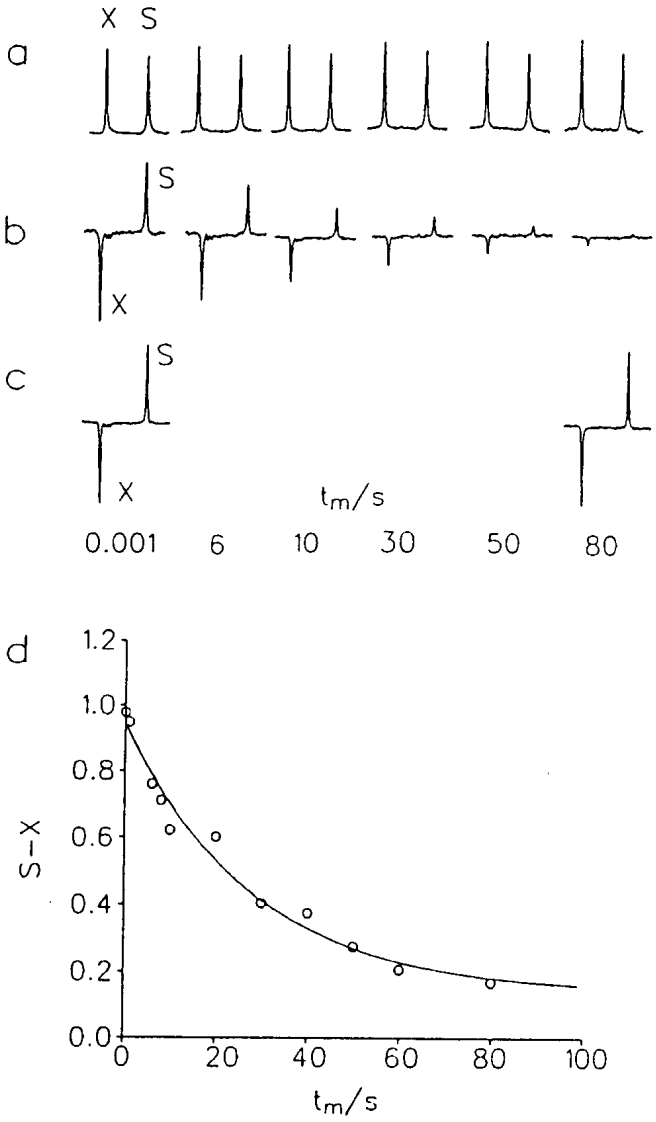

Fig. 7
30.41 MHz ^{15}N CPMAS magnetization transfer experiment in the laboratory frame performed on a sample of singly ^{15}N-labeled DMP at 131 K. (a) Experiment (i) at $x_D = 0$. The two magnetizations S (amino nitrogen sites) and X (imino nitrogen sites) are parallel and decay in the mixing period t_m with the longitudinal ^{15}N relaxation time T_1 which is here of the order of seconds. (b) Experiment (ii) at $x_D = 0$. The magnetizations are antiparallel and their difference decays with the rate constant $2k^{HHH}$ as spin diffusion can be neglected. (c) Experiment (ii) and $x_D = 0.99$. (d) Analysis of the data of Fig. 7c

data of Fig. 7b is shown in Fig. 7d where a mono-exponential decay is observed from which k^{HHH} is obtained.

3.2.2 Determination of k^{HHD} and k^{HDD}

In Fig. 8 are shown the results of experiment (ii) performed at 210 K on two singly ^{15}N-labeled DMP samples (a) with $x_D = 0.2$ ($x_{HHH}:x_{HHD}:x_{HDD}:x_{DDD} = 0.512:0.384:0.096:0.08$) and (b) with $x_D = 0.8$ ($x_{HHH}:x_{HHD}:x_{HDD}:x_{DDD} = 0.008:0.096,\ 0.384:0.512$). Bi-exponential decays are observed in both cases. Whereas in Fig. 8a the fast decay is determined by $2k^{HHH}$ the slow decay is governed by $2k^{HHD}$. The contribution of k^{HDD} could by neglected because of the small value of D_{HDD} i.e. of x_{HDD} at $x_D = 0.2$. On the other hand, in Fig. 8b also a bi-exponential decay is observed determined by $2k^{HDD}$ and $2k^{DDD}$. Here, D_{HHD} could be neglected. We note that the values of k^{HHH} and k^{DDD} do not depend on the deuterium fraction within the margin of error, which corroborates the assumption that the rate constant of triple hydron transfer in a given trimer is independent of the deuterium fraction in the surrounding trimers.

3.3 Arrhenius Diagram

The Arrhenius diagram containing all the rate constant data for the proton and deuteron transfer in the different DMP species is shown in Fig. 9. Especially in the HHH and the HHD reaction deviations from a classical Arrhenius behavior were found. The solid lines in Fig. 9 were calculated in terms of a modified Bell tunneling model as described in the next section.

4. Discussion

Using solid state ^{15}N NMR under CPMAS conditions, in particular line-shape analysis and magnetization transfer experiments we have followed the degenrate triple hydron transfer (Fig. 2c) in the cyclic trimers of polycrystalline singly and doubly ^{15}N-labeled 3,5-dimethylpyrazole (DMP). Partially deuterated DMP represents a statistical mixture of isotopomeric trimers with the mobile particle combinations HHH, HHD, HDD and DDD within the margin of error. The exchange kinetics of a given isotopomeric trimer is independent of the isotopic composition of the neighboring trimers. The kinetic HHH/HHD/HDD/DDD isotope effects were measured in a large temperature interval; for this purpose the problem of signal intensity distortions arising in CPMAS experiments had to be solved. The problem of ^{15}N spin diffusion was solved by ^{15}N isotopic dilution. The kinetic isotope effects are large and the Arrhenius curves of the isotopic reactions exhibit large deviations from a linear behavior (Fig. 9), as was suggested previously [7c]. As multiple hydrogen/deuterium isotope effects have not yet been studied before neither experimentally nor theoretically we discuss in the first part of this section the question of how different reaction mechanisms can influence these isotope effects. In the

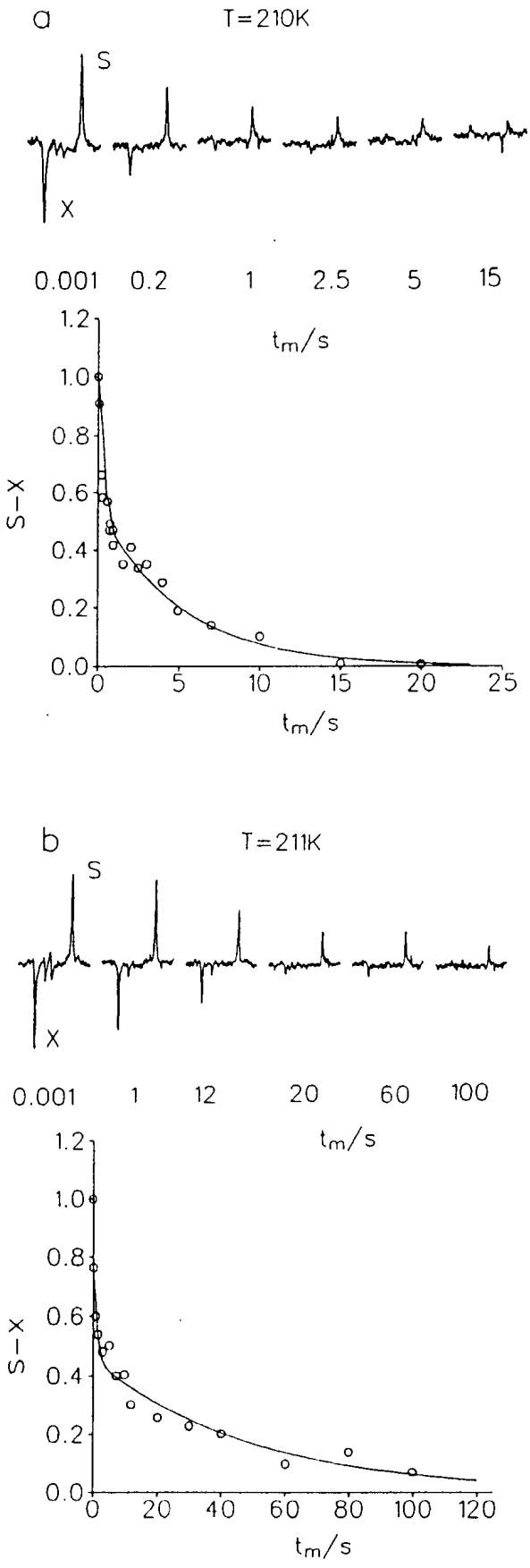

Fig. 8
30.41 MHz ^{15}N CPMAS magnetization transfer experiments (ii) and in the laboratory frame performed on an undiluted sample of singly ^{15}N-labeled DMP at 210 K. (a) $x_D = 0.2$. The fast decay is determined by k^{HHH} and the slow decay by k^{HHD}. (b) $x_D = 0.8$. The fast decay is determined by k^{HDD} and the slow decay by k^{DDD}. All rate constants were obtained by non-linear least squares fitting using Eq. (3)

second part these predictions are applied to the case of DMP.

4.1 Kinetic HHH/HHD/HDD/DDD Isotope Effects of Degenerate Triple Hydron Transfers

The transfer of three hydrons can take place either in three steps each characterized by an energy barrier or in a single step. The two cases are illustrated in Figs. 10 and 11. As each hydron can occupy two positions in space labeled as 0 and 1, the initial and final tautomeric states can be characterized by the digits 000 and 111. The stepwise process leads to the reaction network of Fig. 10a. The reaction can take place in many different ways via at least two metastable intermediates. For example, if hydrons 1, 2, and 3 are transferred one after the other the reaction pathway is 000→100→110→111. As we consider a degenerate reaction the reaction energy profile must be symmetric, leaving only two cases: in the first case (Fig. 10b) the central reaction step is rate limiting and in the second case (Fig. 10c) the first and the third steps.

Expressions for the kinetic isotope effects of the triple barrier case can be evaluated for a given temperature using formal kinetics as shown in the Appendix, without assumptions concerning an over-barrier reaction or a tunneling mechanism. For this case we obtain – neglecting secondary kinetic and equilibrium isotope effects – for both types of barriers in Fig. 10b and c

$$k^{HHH}/k^{HHD} = 3/(2+P^{-1}) \ , \tag{7a}$$

$$k^{HHD}/k^{HDD} = (2+P^{-1})/(1+2P^{-1}) \ , \tag{7c}$$

$$k^{HDD}/k^{DDD} = (P+2)/3 \ , \tag{7b}$$

$$k^{HHH}/k^{DDD} = P \tag{7d}$$

where P represents the primary kinetic H/D isotope effect. Assuming an over-barrier reaction, i.e. Arrhenius laws and similar pre-exponential factors for the H and D transfer one obtains

$$P = (A^H \exp(-E^H/RT))/(A^D \exp(-E^D/RT))$$
$$\approx \exp(-\Delta\varepsilon/RT) \ , \quad \Delta\varepsilon = E^D - E^H \ . \tag{8}$$

$\Delta\varepsilon$ represents the difference of the effective barriers of the H and D transfer, and is essentially given by the loss of zero-point energy in the transition state as compared to the initial state, as illustrated in Fig. 10b and c. Using Eqs. (7) and (8) and an arbitrary value of $\Delta\varepsilon$ we obtain the Arrhenius curves of Fig. 10d. At high temperatures P is close to 1 and all isotope effects in Eq. (7) are unity. At low temperatures $P \gg 1$, but according to Eq. (7), a substantial temperature-dependent kinetic isotope effect is predicted only for the replacement of all three protons by deuterons. This result is astonishing at first sight, but can be made plausible as follows. When the central step is rate limiting either a H is transferred in this step with the probability 1/3 or a D with the probability 2/3. The latter D transfer does not contribute substantially to the overall rate constant, as the reaction where H is transferred in the central step is as fast as a single HHH reaction sequence. Therefore, the HHH/HHD and the HHD/HDD isotope effects are constant and given only by statistical factors. When the outer reaction steps are rate limiting and the central step fast, a similar phenomenon occurs, as in the HDD reaction there are sequences where the remaining H is transferred both in the first and the final rate limiting steps, e.g. the sequence 000→100→101→001→011→111. Therefore, also in this case only replacement of the last proton by a deuteron exhibits a non-statistical kinetic isotope effect.

In Fig. 11a is depicted the reaction energy profile of the single barrier case where all three hydrons are transferred

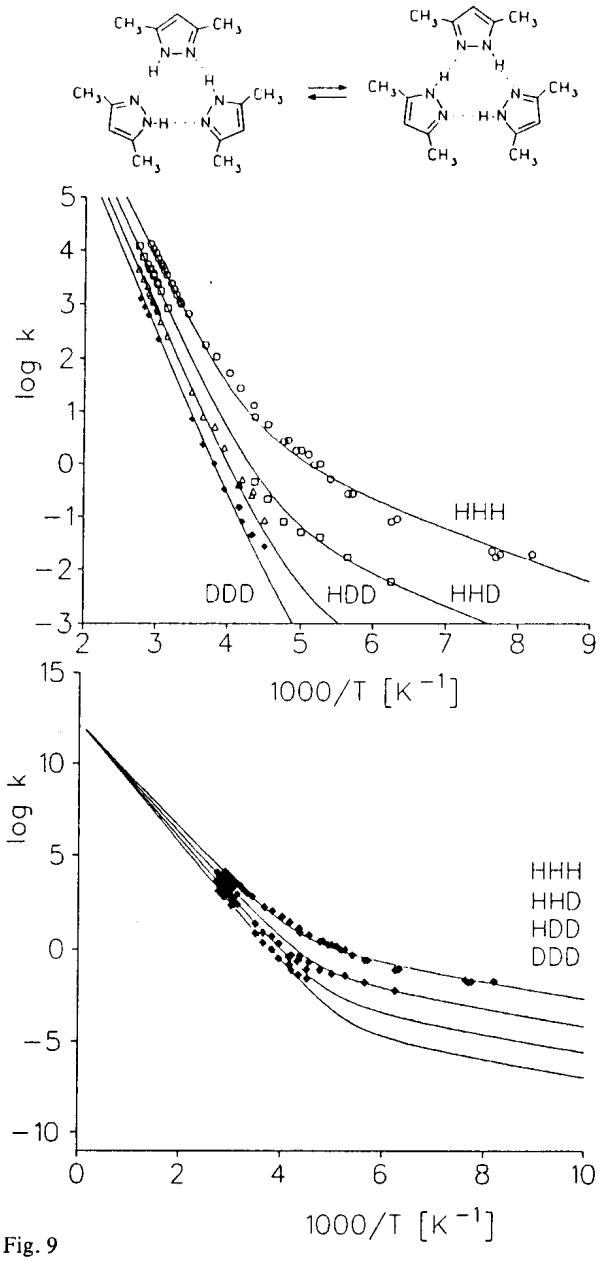

Fig. 9
Arrhenius diagram for the triple proton and deuteron transfer in solid DMP. The solid curves were calculated using a modified Bell tunneling model as described in the text

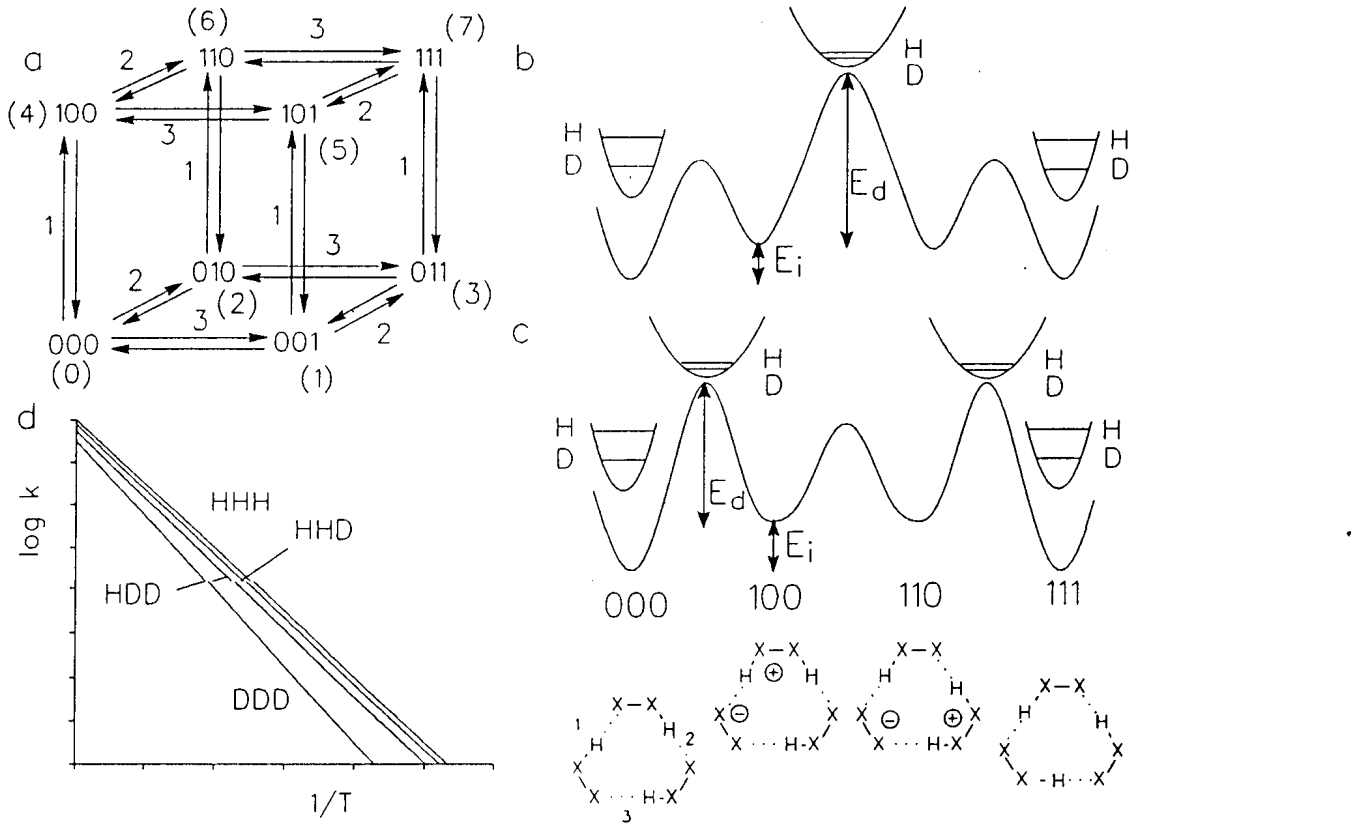

Fig. 10
(a) Reaction network of a stepwise degenerate triple hydron transfer. If each hydron occupies two positions labeled as 0 and 1, each tautomeric state can be characterized by three digits. (b) and (c) Examples of one-dimensional reaction energy profiles along the pathway 000-100-110-111 involving consecutive barriers. The zero-point energies of the hydron transferred are illustrated schematically for the initial, final and the transition states. (d) Arrhenius curves of the various isotopic processes calculated in terms of Eqs. (7) and (8) using arbitrary parameters

together. In the literature of isotope effects often the so-called rule of the geometric mean (RGM) has been assumed to be valid in the case where several proton by a deuteron involves the same primary isotope effect P. Here, this rule would predict that

$$k^{HHH}/k^{HHD} = k^{HHD}/k^{HDD} = k^{HDD}/k^{DDD} = P \ ,$$
$$k^{HHH}/k^{DDD} = P^3 \qquad (9)$$

where P is given by Eq. (8). This rule is valid if the kinetic isotope effects are only given by losses of zero-point energies in the transition state and if each hydron looses the same energy $\Delta\varepsilon$ as is illustrated in Fig. 11a. Using Eqs. (8) and (9) and the same value $\Delta\varepsilon$ as in Fig. 10d we obtain the Arrhenius diagram of Fig. 11b, exhibiting equally spaced Arrhenius curves for the various isotopic reactions. In summary, for given values of P or $\Delta\varepsilon$ the kinetic HHH/DDD isotope effects are much larger in the single barrier case as compared to the triple barrier case.

The energy reaction profiles of Fig. 10b and c and of Fig. 11a only consider the hydron motion but not an associated heavy atom motion. In order to obtain information about this problem some of us have performed ab initio calculations on multiple proton transfers in cyclic pyrazole dimers, trimers and tetramers [7p] and have obtained qualitative evidence for an energy surface of the type shown in Fig. 11c, where the concerted transfer of the three protons characterized by the distance r_{XH} is associated with a concerted hydrogen bond compression characterized by the heavy atom distance $r_{X\cdots X}$. Naturally, this two-dimensional surface is also only an approximation as it does not include for example the reorganization of the molecular skeletons i.e. single-double bond shifts during the transfer, or molecular librations. Within the framework of this approximation, the one-dimensional reaction coordinate in Fig. 11a corresponds to the dotted line linking the initial and final states A and A′ via the transition state B. This pathway will be realized only at high temperature; at lower temperatures one also has to consider direct "horizontal" trajectories corresponding to hydron tunneling at constant heavy atom distances $r_{X\cdots X}$. Unfortunately, the problem of multidimensional tunneling is very difficult and beyond the scope of this study, and even more complicated in the case of the triple barrier case.

Therefore, in order to interpret the experimental kinetic data obtained in this study we use here the simplest possible approach, i.e. the single particle one-dimensional tunnel model proposed by Bell [9]. This model assumes a single inverted parabola as energy barrier and a continuous distribution of vibrational states on both sides of the barrier of the single hydron transfer. In this model Eq. (8) is replaced by

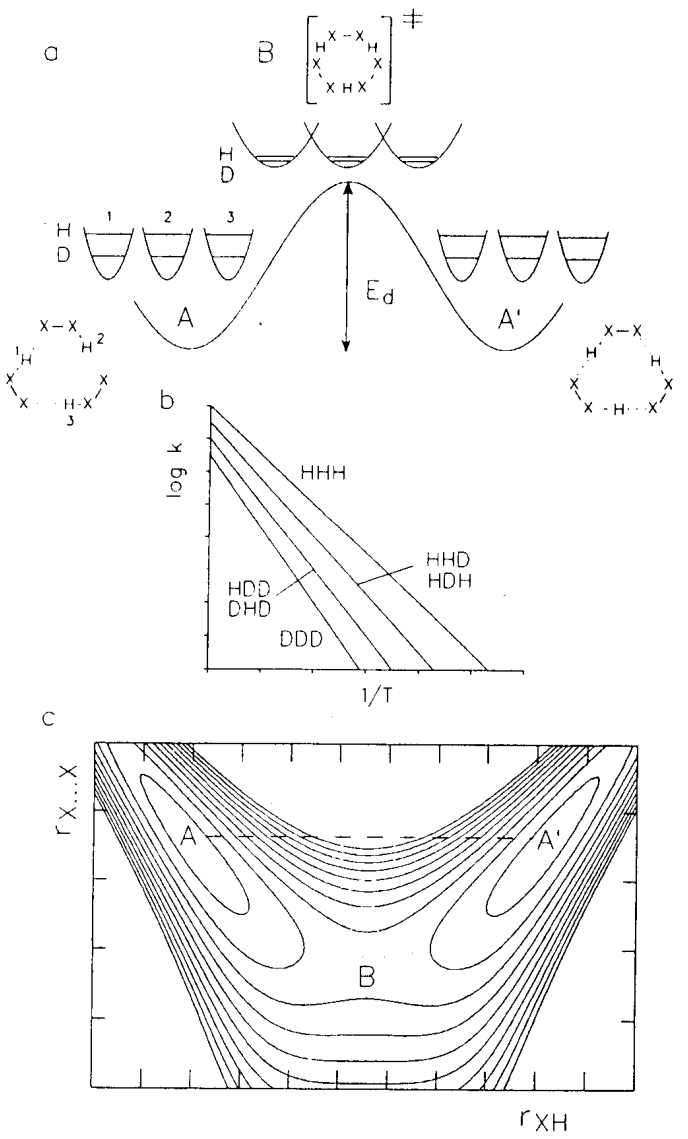

Fig. 11
(a) One-dimensional reaction energy profile (schematically) for a degenerate single barrier (concerted) triple hydron transfer. (b) Arrhenius curves of a degenerate triple hydron transfer assuming the single barrier case (concerted process), calculated using Eqs. (8) and (9), i.e. using the rule of the geometric mean. (c) Two-dimensional energy reaction surface involving a reduction of the all heavy atom distances $r_{X\cdots X}$ prior to the hydron transfer, as proposed by ab initio calculations [7p]. Points A and A' correspond to the states 000 and 111, and B corresponds to the transition state where the zero-point energies of all hydrons are reduced as indicated in Fig. 7a. The minimum energy pathway (dashed curve) involves a substantial hydrogen bond compression and an associated gradual shift of the hydron

$$P = k^H/k^D = (A^H Q^H \exp(-E^H/RT))/(A^D Q^D \exp(-E^D/RT)) , \quad (10)$$

where Q^H and Q^D represent tunnel corrections. This model was modified by some of us in recent years [1, 3, 4]. For a detailed description of the expressions of the tunnel corrections as a function of various barrier parameters the reader is referred to the literature. Here, we included the following adjustable parameters:

(i) $E_m = E_r + E_i$ represents a minimum energy for tunneling to occur, and is assumed to be isotope independent. E_r represents a contribution arising from heavy atom reorganization *preceding* the hydron tunneling process at $T = 0$. E_i represents the energy of a possible intermediate and is zero in the single barrier case.

(ii) E_d^{HHH} is the barrier height for the proton transfer; it does not include E_m which adds up to the total barrier height.

(iii) $\Delta\varepsilon$ is defined in Eq. (8) and represents the increase of the barrier height a single H is replaced by D. In other words, in the case of the stepwise single hydron processes $\Delta\varepsilon = E_d^H - E_d^D$ and in the concerted process $\Delta\varepsilon = E_d^{HHD} - E_d^{HHH} = E_d^{HDD} - E_d^{HHD} = E_d^{DDD} - E_d^{HDD}$. This assumption is responsible for the validity of the RGM (Eq. (9)) at high temperatures.

(iv) $2a$ is the barrier width of the H transfer in Å at the energy E_m.

(v) A single frequency factor A in s^{-1} is used for all isotopic reactions, i.e. a possible mass dependence [9] is neglected within the margin of error.

(vi) The tunneling masses are given in the stepwise case by $m_{eff}^L = m^L + \Delta m$, L = H, D, and in the concerted case by $m_{eff}^{LLL} = m^{LLL} + \Delta m$, with the fixed values $m^H = 1$, $m^D = 2$, $m^{HHH} = 3$, $m^{HHD} = 4$, $m^{HDD} = 5$, $m^{DDD} = 6$. Δm takes into account the possibility of small heavy atom displacements during the tunnel process.

4.2 Mechanism of Triple Hydron Transfer in DMP

The kinetic data of the triple hydron transfer in DMP assembled in Fig. 9 indicate that the rule of the geometric mean (Eq. (9)) is fulfilled within the margin of error in the temperature range $300 \leq T \leq 364$ K. E.g., at 300 K we find that $k^{HHH}/k^{DHH} \approx k^{DHH}/k^{DDH} \approx k^{DDH}/k^{DDD} \approx 3.6$ and $k^{HHH}/k^{DDD} = (3.6)^3 \approx 47$. This high-temperature isotope effect is ascribed to the loss of a similar zero-point energy $\Delta\varepsilon$ of each hydron in the transition states. Thus, the experimental kinetic data in the high temperature regime support the triple but not the single barrier mechanism.

At lower temperatures, deviations from the rule of geometric mean are observed, as indicated in Fig. 9, and a non-Arrhenius behavior of the various isotopic rate constants which can be ascribed to hydron tunneling. The solid lines in Fig. 9 were fitted to the experimental data in terms of the single barrier case using a non-linear least squares fitting procedure, varying the above-mentioned barrier parameters. The agreement between experimental and calculated rate constants is satisfactory. The parameters obtained are assembled in Table 5. They are all plausible, but their physical significance should not be overestimated, in view of the many approximations used in this model. Noteworthy is the additional tunneling mass of $\Delta m = 0.5$ which indicates a small heavy atom tunneling contribution. This contribution could arise either from the reorganization of the pyrazole skeleton or from a small angle reorientation of the whole pyrazole units *during* the hydron tunnel process.

As a result, a single barrier (concerted) reaction mechanism for the triple hydron transfer in solid DMP

Table 5
Parameters of the modified Bell model of the triple hydron transfer in polycrystalline 3,5-dimethylpyrazole

	E_d	E_m	E_d+E_m	$\log A$	$2a$	$\Delta\varepsilon$	Δm
DMP	48.1	8.4	56.5	12.3	0.70	1.5	0.5

Barrier height E_d and minimum energy for tunneling E_m in kJ mol^{-1}, $\Delta\varepsilon$ additional barrier energy for replacing one H by D in kJ mol^{-1}, barrier width $2a$ in Å, frequency factor A in s^{-1}. Tunneling masses $m_{eff}^{LLL} = m^{LLL} + \Delta m$, $m^{HHH} = 3$, $m^{HHD} = 4$, $m^{HDD} = 5$, $m^{DDD} = 6$ (fixed)

results from the following observations: (i) the rule of the geometric mean is fulfilled at high temperatures; (ii) the kinetic HHH/DDD isotope effects are very large even above room temperature; (iii) the Arrhenius curves of all isotopic reactions can be accommodated by the simple modified Bell tunneling model where the transfer of a hydron triple LLL = HHH, or HHD, or HDD or DDD is treated as a single particle transfer process. The single barrier mechanism is supported by recent ab initio calculations and is assisted by hydrogen bond compression [7p] (Fig. 11c). This is because in the cyclic DMP trimers the hydrogen bonds are cooperative in the sense that compression of any hydrogen bond induces also the compression of the other hydrogen bonds. As has been discussed previously in the case of double proton transfer reactions [1–4], a stepwise process is preferred when the hydrogen bonds can not easily be compressed – as is often the case in compounds of the porphyrin type – or when they are anticooperative as in the case of oxalamidines. Here, compression of one bond leads to a widening of the other bond ending in a stepwise double proton transfer pathway.

The correlation of the heavy atom distance $r_{X\cdots X}$ with the proton transfer distance r_{XH} along the minimum energy pathway of Fig. 11c is independently supported by analysis of the neutron diffraction geometries of a number of crystals exhibiting N-H···N hydrogen bonds by Steiner [17], as well as by low-temperature liquid state NMR [18] of various acid base complexes between pyridine and carboxylic acids. Here, the various configurations are static and produced by structural changes. The loss of zero-point energy of the hydron motion is then not so much due to the breaking of the N-H bonds, but due to the low frequency shift of the NH-stretching vibration during the compression of the hydrogen bond.

5. Conclusions

The full multiple kinetic HHH/HHD/HDD/DDD isotope effects of a triple proton transfer reaction have been measured in the case of 3,5-dimethylpyrazole by variable temperature solid state NMR methods and modeled with a single barrier process involving a strong hydrogen bond compression in the transition state, and a concerted triple proton tunneling process at low temperatures. The isotope effects were described theoretically using a simplified Bell tunneling model. In the future, it would be desirable to apply multi-dimensional tunneling models in connection with ab initio calculations to this kind of reaction; in other words, the data obtained here could serve for the test of improved theoretical models of proton transfer. Currently, we are trying to study the isotope effects of related double and quadruple proton transfer processes in solid pyrazoles in order to evaluate the influence of the number of hydrons transferred.

6. Appendix

In this section we want to give an outline for the derivation of Eq. (7) valid for the reaction network of Fig. 10a. In each reaction step one of the hydrons 1, 2 or 3 = H or D changes its position, leading to an interconversion from state $i = 000(\equiv 0), \ldots 111(\equiv 7)$ to another state j. The three digit nomenclature has the advantage that it encodes the number of the jumping hydron. Each state is characterized by the concentration c_i, and the interconversion between i and j by the rate constants k_{ij}. Only the initial and the final states are significantly populated, and the other states are treated as metastable intermediates for which the usual steady state approximation is fulfilled. The set of differential equations describing this reaction network is then given by

$$\frac{dc_0}{dt} = -k_{01}c_0 - k_{02}c_0 - k_{04}c_0 + k_{10}c_1 + k_{20}c_2 + k_{40}c_4 \,, \tag{A1a}$$

$$\frac{dc_1}{dt} = -k_{10}c_1 - k_{13}c_1 - k_{15}c_1 + k_{01}c_0 + k_{31}c_3 + k_{51}c_5 = 0 \,, \tag{A1b}$$

$$\frac{dc_2}{dt} = -k_{20}c_2 - k_{26}c_2 - k_{23}c_2 + k_{02}c_0 + k_{32}c_3 + k_{62}c_6 = 0 \,, \tag{A1c}$$

$$\frac{dc_3}{dt} = -k_{31}c_3 - k_{32}c_3 - k_{37}c_3 + k_{13}c_1 + k_{23}c_2 + k_{73}c_7 = 0 \,, \tag{A1d}$$

$$\frac{dc_4}{dt} = -k_{40}c_4 - k_{45}c_4 - k_{46}c_4 + k_{04}c_0 + k_{54}c_5 + k_{64}c_6 = 0 \,, \tag{A1e}$$

$$\frac{dc_5}{dt} = -k_{51}c_5 - k_{54}c_5 - k_{57}c_5 + k_{15}c_1 + k_{45}c_4 + k_{75}c_7 = 0 \,, \tag{A1f}$$

$$\frac{dc_6}{dt} = -k_{62}c_6 - k_{64}c_6 - k_{67}c_6 + k_{26}c_2 + k_{46}c_4 + k_{76}c_7 = 0 \,, \tag{A1g}$$

$$\frac{dc_7}{dt} = -k_{73}c_7 - k_{75}c_7 - k_{76}c_7 + k_{37}c_3 + k_{57}c_5 + k_{67}c_6 \,. \tag{A1h}$$

This set of equations reduces to

$$\frac{dc_0}{dt} = -k_{07}c_0 + k_{70}c_7 \,, \tag{A2}$$

where k_{07} and k_{70} are the observed rate constants. The analytical solution Eq. (A2) can be written as

$$k_{07} = k_{67}(b + cr + dp)/a + k_{57}r + k_{37}p \,, \tag{A3a}$$

$$p = ((af+gb)(an+mc) + (at+mb)(ae-gc))/(as-md)(ae-gc) - (ak+gd)(an+mc)) \,, \tag{A3b}$$

$$r = p((af+gb)(ak+gd))/(ae-gc)^2 \,, \tag{A3c}$$

$$a = k_{64} + k_{62} + k_{67} - k_{46}k_{64}/(k_{40}+k_{46}+k_{45}) - k_{26}k_{62}/(k_{20}+k_{26}+k_{23}) \,, \tag{A3d}$$

$$e = k_{54} + k_{51} + k_{57} - k_{45}k_{54}/(k_{40} + k_{46} + k_{45}) - k_{15}k_{51}/(k_{10} + k_{15} + k_{13}) \ , \tag{A3e}$$

$$s = k_{32} + k_{31} + k_{37} - k_{23}k_{32}/(k_{20} + k_{26} + k_{23}) - k_{13}k_{31}/(k_{10} + k_{15} + k_{13}) \ , \tag{A3f}$$

$$b = k_{04}k_{46}/(k_{40} + k_{46} + k_{45}) - k_{02}k_{20}/(k_{20} + k_{26} + k_{23}) \ , \tag{A3g}$$

$$f = k_{04}k_{45}/(k_{40} + k_{46} + k_{45}) - k_{01}k_{15}/(k_{10} + k_{15} + k_{13}) \ , \tag{A3h}$$

$$t = k_{02}k_{23}/(k_{20} + k_{26} + k_{23}) + k_{01}k_{13}/(k_{10} + k_{15} + k_{13}) \ , \tag{A3i}$$

$$c = k_{46}k_{54}/(k_{40} + k_{46} + k_{45}), \ d = k_{26}k_{32}/(k_{20} + k_{26} + k_{23}),$$
$$g = k_{45}k_{64}/(k_{40} + k_{46} + k_{45}) \ , \tag{A3j}$$

$$h = k_{15}k_{31}/(k_{10} + k_{15} + k_{13}), \ m = k_{23}k_{62}/(k_{20} + k_{26} + k_{23}),$$
$$n = k_{13}k_{51}/(k_{10} + k_{15} + k_{13}) \ . \tag{A3k}$$

In order to derive Eq. (7) we neglect equilibrium isotope effects, i.e. we set

$$P_{ij} = k_{ij}^{(H)}/k_{ij}^{(D)} = k_{ji}^{(H)}/k_{ji}^{(D)} \ . \tag{A4}$$

As Eq. (7) refers to the degenerate case it follows that $k_{07} = k_{70} = k$. This constant must be evaluated separately for the hydron triples (1)(2)(3) = HHH, HHD, HDD and DDD. This is simplified by taking into account the symmetry of the reaction profile in the case of the HHH and the DDD transfer where

$$k_{12} = k_{13} = k_{14} = k_{73} = k_{75} = k_{76} \ , \tag{A5a}$$

$$k_{21} = k_{31} = k_{41} = k_{37} = k_{57} = k_{67} \ , \tag{A5b}$$

$$k_{15} = k_{51} = k_{45} = k_{54} = k_{46} = k_{64} = k_{62} = k_{26} = k_{23} = k_{32} = k_{12} = k_{21} \ . \tag{A5c}$$

For the reaction profile of Fig. 10b where $k_{10} \gg k_{15}$ etc. we obtain

$$k = K(k_{46}^{(2)} + k_{45}^{(3)} + k_{26}^{(1)} + k_{23}^{(3)} + k_{15}^{(1)} + k_{13}^{(2)}) \ , \tag{A6}$$

where the superscript indicates the number of the jumping hydron H or D and where

$$K = k_{01}^{(H)}/k_{10}^{(H)} = k_{01}^{(D)}/k_{10}^{(D)} \tag{A7}$$

is isotope independent. By setting (1)(2)(3) = HHH, HHD, HDD, and DDD in Eq. (A6) and taking into account Eqs. (A4) and (A5) Eq. (7) can be derived in a straightforward way. The validity of Eq. (7) for the case of Fig. 10c is demonstrated in a similar way by setting $k_{10}^{(L)} \ll k_{15}^{(L)}$.

The funding of the following institutions is gratefully acknowledged: Deutsche Forschungsgemeinschaft (Bad Godesberg), Fonds der Chemischen Industrie (Frankfurt), European Network Human Capital & Mobility on "Localization and Transfer of Hydrogen" (Brussels).

References

[1] a) H.H. Limbach, J. Hennig, R.D. Kendrick, and C.S. Yannoni, J. Am. Chem. Soc. *106*, 4059 (1984); b) R.D. Kendrick, S. Friedrich, B. Wehrle, H.H. Limbach, and C.S. Yannoni, J. Magn. Reson. *30*, 159 (1985); c) B. Wehrle, H.H. Limbach, M. Köcher, O. Ermer, and E. Vogel, Angew. Chem. *99*, 914 (1987); Angew. Chem. Int. Ed. *26*, 934 (1987); d) H.H. Limbach, B. Wehrle, H. Zimmermann, R.D. Kendrick, and C.S. Yannoni, J. Am. Chem. Soc. *109*, 929 (1987); e) H.H. Limbach, B. Wehrle, H. Zimmermann, R.D. Kendrick, and C.S. Yannoni, Angew. Chem. *99*, 241 (1987); Angew. Chem. Int. Ed. Eng. *26*, 247 (1987); f) B. Wehrle, H.H. Limbach, and H. Zimmermann, Ber. Bunsenges. Phys. Chem. *91*, 941 (1987); g) H.H. Limbach, B. Wehrle, M. Schlabach, R.D. Kendrick, and C.S. Yannoni, J. Magn. Reson. *77*, 84 (1988); h) B. Wehrle, H. Zimmermann, and H.H. Limbach, J. Am. Chem. Soc. *110*, 7014 (1988); i) B. Wehrle and H.H. Limbach, Chem. Phys. *136*, 223 (1989); j) M. Schlabach, B. Wehrle, J. Braun, G. Scherer, and H.H. Limbach, Ber. Bunsenges. Phys. Chem. *96*, 821 (1992); k) J. Braun, M. Schlabach, B. Wehrle, M. Kröger, E. Vogel, and H.H. Limbach, J. Am. Chem. Soc. *116*, 6593 (1994); l) C.G. Hoelger, B. Wehrle, H. Benedict, and H.H. Limbach, J. Phys. Chem. *98*, 843 (1994).

[2] a) J. Braun, H.H. Limbach, P. Williams, H. Morimoto, and D. Wemmer, J. Am. Chem. Soc. *30*, 7231 (1996); b) J. Braun, R. Schwesinger, P.G. Williams, H. Morimoto, D.E. Wemmer, and H.H. Limbach, J. Am. Chem. Soc., im Druck.

[3] a) H.H. Limbach, Dynamic NMR Spectroscopy in the Presence of Kinetic Hydrogen Deuterium Isotope Effects, Chap. 2, in: NMR Basic Principles and Progress, Vol. 26, Springer, Berlin Heidelberg New York 1991; b) H.H. Limbach, G. Scherer, L. Meschede, F. Aguilar-Parrilla, B. Wehrle, J. Braun, C. Hoelger, H. Benedict, G. Buntkowsky, W.P. Fehlhammer, J. Elguero, J.A.S. Smith, and J.B. Chaudret, NMR Studies of Elementary Steps of Hydrogen Transfer in Condensed Phases, in: Y. Gauduel and P.J. Rossky (eds.) Ultrafast Reaction Dynamics and Solvent Effects, American Institute of Physics, AIP Conference Proceedings, Part III, *298*, 225 – 239 (1994).

[4] a) D. Gerritzen and H.H. Limbach, J. Am. Chem. Soc. *106*, 869 (1984); b) H. Rumpel and H.H. Limbach, J. Am. Chem. Soc. *111*, 5429 (1989); c) G. Scherer and H.H. Limbach, J. Am. Chem. Soc. *111*, 5946 (1989); d) L. Meschede and H.H. Limbach, J. Phys. Chem. *95*, 10267 (1991); e) G. Scherer and H.H. Limbach, J. Am. Chem. Soc. *113*, 1230 (1994); f) G. Scherer and H.H. Limbach, Croatica Chimica Acta *67*, 431 (1994); g) L. Meschede, D. Gerritzen, and H.H. Limbach, Ber. Bunsenges. Phys. Chem. *92*, 496 (1988); h) H.H. Limbach, L. Meschede, and G. Scherer, Z. Naturforsch. *44a*, 459 (1989).

[5] a) B.H. Meier, F. Graf, and R.R. Ernst, J. Chem. Phys. *76*, 768 (1982); b) R. Meyer and R.R. Ernst, J. Chem. Phys. *93*, 5518 (1990); c) A. Stöckli, B.H. Meier, R. Kreis, R. Meyer, and R.R. Ernst, J. Chem. Phys. *93*, 1502 (1990); d) A. Heuer and U. Haeberlen, J. Chem. Phys. *95*, 4201 (1995).

[6] F. Männle, I. Wawer, and H.H. Limbach, Chem. Phys. Lett. *256*, 657 (1996).

[7] a) A. Baldy, J. Elguero, R. Faure, M. Pierrot, and F.J. Vincent, J. Am. Chem. Soc. *107*, 5290 (1985); b) J.A.S. Smith, B. Wehrle, F. Aguilar-Parrilla, H.H. Limbach, M.C. Foces-Foces, F.H. Cano, J. Elguero, A. Baldy, M. Pierrot, M.M.T. Khurshid, and J.B. Larcombe-McDouall, J. Am. Chem. Soc. *111*, 7304 (1989); c) F. Aguilar-Parrilla, H.H. Limbach, M. Blanz, T.J. Rayner, and J.A.S. Smith, Magn. Reson. Rel. Phenomena *25*, 615 (1990); d) F. Aguilar-Parrilla, C. Cativiela, M.D. Diaz de Villegas, J. Elguero, M.C. Foces-Foces, J.I.G. Laureiro, F.H. Cano, H.H. Limbach, J.A.S. Smith, and C. Toiron, J. Chem. Soc. Perkin *2*, 1737 (1992); f) F. Aguilar-Parrilla, G. Scherer, H.H. Limbach, M.C. Foces-Foces, F.H. Cano, J.A.S. Smith, C. Toiron, and J. Elguero, J. Am. Chem. Soc. *114*, 9657 (1992); g) F. Toda, K. Tanaka, M.C. Foces-Foces, A.L. Llamas-Saiz, H.H. Limbach, F. Aguilar-Parrilla, R.M. Claramunt, C. Lopez, and J. Elguero, J. Chem. Soc. Chem. Comm. 1139 (1993); h) F. Aguilar-Parrilla, R.M. Claramunt, C. Lopez, D. Sanz, H.H. Limbach, and J. Elguero, J. Phys. Chem. *98*, 8752 (1994); i) J. Elguero, F.H. Cano, M.C. Foces-Foces, A.L. Llamas-Saiz, H.H. Limbach, F. Aguilar-Parrilla, R.M. Claramunt, and C. Lopez, J. Heterocycl. Chem. *31*, 695 (1994); j) F. Aguilar-Parrilla, F. Männle, H.H. Limbach, J. Elguero, and N. Jagerovic, Magn. Reson. Chem. *32*, 699 (1994); k) A.L. Llamas-Saiz, M.C. Foces-Foces, F.H. Cano, J. Elguero, P. Jimenez, J. Laynez, W. Meutermans, J. Elguero, H.H. Limbach, and F. Aguilar-Parrilla, Acta Crystallogr. *B50*, 746 (1994); l) F. Aguilar-Parrilla, H.H. Limbach, M.C. Foces-Foces, F.H. Cano, N. Jagerovic, and J. Elguero, J. Org. Chem. *60*, 1965 (1995); m) J. Elguero, N. Jagerovic, M.C. Foces-Foces, F.H. Cano, M.V. Roux, F. Aguilar-Parrilla, and H.H. Limbach,

J. Heterocyclic Chem. *32*, 451 (1995); n) C.G. Hoelger, H.H. Limbach, F. Aguilar-Parrilla, J. Elguero, O. Weintraub, and S. Vega, J. Magn. Res. *A120*, 46 (1996); o) C. Lopez, R.M. Claramunt, A. Llamas-Saiz, M.C. Foces-Foces, J. Elguero, I. Sobrados, F. Aguilar-Parrilla, and H.H. Limbach, New J. Chem. *20*, 523 (1996); p) J.L.G. de Paz, J. Elguero, M.C. Foces-Foces, A. Llamas-Saiz, F. Aguilar-Parrilla, O. Klein, and H.H. Limbach, J. Chem. Soc. Perkin Trans. *2*, 101 (1997).

[8] a) M.A. Suhm, Ber. Bunsenges. Phys. Chem. *99*, 1159 (1995); b) M. Quack and M.A. Suhm, Theor. Chim. Acta *93*, 61 (1996).

[9] a) R.P. Bell, The Tunnel Effect, 2nd ed., Chapman and Hall, London 1980; b) E. Caldin and V. Gold, Proton Transfer, Chapman and Hall, London 1975; c) L. Melander and W.H. Saunders, Reaction Rates of Isotopic Molecules, John Wiley & Sons, New York Toronto 1980.

[10] a) N.M. Szeverenyi, M.J. Sullivan, and G.E. Maciel, J. Magn. Reson. *47*, 462 (1982); b) P. Caravatti, J.A. Deli, G.R. Bodenhausen, and R.R. Ernst, J. Am. Chem. Soc. *104*, 5506 (1982); c) M. Linder, P.M. Henrichs, J.M. Hewitt, and D.J. Massa, J. Chem. Phys. *82*, 1585 (1985); d) P.M. Henrichs, M. Linder, and J.M. Hewitt, J. Chem. Phys. *85*, 7077 (1986); e) D. Suter and R.R. Ernst, Phys. Rev. B *32*, 5608 (1985); f) P. Robyr, B.H. Meier, and R.R. Ernst, Chem. Phys. Lett. *162*, 417 (1989).

[11] R.H. Wiley and P.E. Hexner, Org. Synth. Collect. *4*, 351 (1963).

[12] B. Bak, C.H. Christensen, D. Christensen, T.S. Hansen, E.J. Pedersen, and J.T. Nielsen, Acta Chem. Scand. *19*, 2434 (1965).

[13] a) F. Aguilar-Parrilla, B. Wehrle, H. Bräunling, and H.H. Limbach, J. Magn. Reson. *87*, 592 (1990); b) B. Wehrle, F. Aguilar-Parrilla, and H.H. Limbach, J. Magn. Reson. *87*, 584 (1990).

[14] R.D. Kendrick, S. Friedrich, B. Wehrle, H.H. Limbach, and C.S. Yannoni, J. Magn. Reson. *65*, 159 (1985).

[15] D. Torchia, J. Magn. Reson. *30*, 613 (1978).

[16] a) C.A. Fyfe, Solid State NMR for Chemists, C.F.C. Press, Guelph, Ontario 1983; b) M. Mehring, Principles of High Resolution NMR in Solids, Springer, Berlin 1983.

[17] a) Th. Steiner and W. Saenger, Acta Crystallogr. *B50*, 348 (1994); b) Th. Steiner, J. Chem. Soc. Chem. Comm. 1331 (1995).

[18] S.N. Smirnov, N.S. Golubev, G.S. Denisov, H. Benedict, P. Schah-Mohammedi, and H.H. Limbach, J. Am. Chem. Soc. *118*, 4094 (1996).

(Received: November 26, 1996 E 9432
final version: February 12, 1997)